Chapter 11

# Fabrication of a Cell Electrostimulator Using Pulse Laser Deposition and Laser Selective Thin Film Removal

Angel Luis Aragón Beloso,
María del Carmen Bao Varela,
Alejandro Fernández Rodríguez, Gerard O'connor,
Eliseo Pérez Trigo, Antonio Pazos Álvarez and
Daniel Nieto García

Additional information is available at the end of the chapter

http://dx.doi.org/10.5772/intechopen.70677

**Abstract**

In this work, we present a laser-based process for fabricating a cell electrostimulator. The fabrication methodology comprises two laser processes: a pulse laser deposition (PLD) of an aluminum thin film on soda-lime glass and a laser-based selectively removal of the thin film. The laser set-up for PLD consist of Nd:$YVO_4$ Rofin Power line 20E (1064 nm wavelength, 20 ns pulse width) focused by a lens of 160 mm focal length inside a vacuum chamber to strike a target of the deposited material. The same laser is used for selectively removing the thin film but focused by a lens of 100 mm focal length. The geometry design is made in CAD-like software. Before microfabrication, a thin aluminum layer (1 μm thickness) is deposited on soda-lime glass using the PLD method. In order to assemble the device, the electrical stimulator is placed between two polycarbonate sheets of 1.5 mm thickness. To prevent any contact with the electric circuit, a thin silicate glass (100 μm) is placed over the electrostimulator. Simulations were performed using ANSYS Maxwell software, verifying that the induced electrical field achieves the minimum for cell stimulation.

**Keywords:** electrical stimulator, PLD, thin film removal, laser ablation, thin film

## 1. Introduction

Electrostimulation is an electric current application method used for excitation and activation of certain organs and systems of the human body [1]. Although many organs and systems can be stimulated by electric currents by adequate methods and techniques applied, the most

widely practiced application is heart electrostimulation, being a specific section of medicine, and electrostimulation of motor nerves and muscles [2].

For electrostimulation, direct impulse currents of different impulse shapes are applied at different duration and frequency. This method is widely used for therapeutic purposes, where the electrical stimulation is used to restore the function of damaged motor nerve, to treat paralysis or muscles restoration while causing motor excitation and contraction of the muscles [3].

Aside from these therapies, where the electric pulses are applied directly to the patient, electrostimulators are used in medical investigation as a tool to induce electric signals in cell cultures simulating different body conditions [4]. In this method, electrostimulators must be carefully designed to work in very specific circumstances. Usually, the device consists of two electrodes in direct contact with the cell culture, where the electric stimulus is induced by applying a voltage between them [5]. In this situation, it is necessary to choose the right material for the electrodes. They must be biocompatible to avoid toxic reactions in the culture and they also must efficiently transfer the charge to the medium in order to minimize the electrode degradation [6].

All these circumstances significantly limit the choice of the materials used in the device [7]. With the purpose of avoiding this problem, we present a design of an electrostimulator in which the electrodes are not in contact with the cell culture, solving the biocompatibility issue, and the stimulation is applied by inducing electric fields, avoiding degradation by electrochemical phenomena. Applications study the growth and information processing of neurons [8], capillary electrophoresis chips for the separation of biochemicals such as amino acids and nucleotides [9], and microstructures for the analysis of DNA [10]. Depending on which types of cells are needed to stimulate, the electrical forces induced can be classified into electrophoresis (EP) or dielectrophoresis (DEP) depending on whether they act on a particle's fixed or induced charge, respectively. In both cases, the electrical field needed to induce notable forces in the cell culture depends on the type of cell, but is usually about $10^4$ V/m [11].

Different techniques have been used in the fabrication of microelectrodes. Most of them are fabricated using standard photolithography [12] because this technique is more versatile and allows the preparation of electrodes with a broad range of shapes and sizes, both single electrodes and the electrode arrays. However, photolithography technique needs usually about 3 h to fabricate planar electrodes, and it demands the use of several components in various steps and the final use of chemical components to remove the additional film.

But in the past decades, pulse laser deposition (PLD) has emerged as one of the most popular, flexible, and simple technique for depositing a wide range of materials [13]. Because of its inherent versatility, flexibility, and speed, this method can be applied to almost any material, from simple metals to multicomponent high-quality single crystals [14].

The PLD technique is a physical vapor deposition process where a pulsed laser is focused on the surface of the material to be deposited as a thin film over a substrate. During the interaction between a laser beam with enough energy density and a target, each laser pulse ablates a small amount of the target, creating a plasma plume where particles of different sizes (form single atoms to clusters) are extracted at high energies from the material. These ejected particles

usually have an initial speed that could reach values of tens of kilometers per second, decreasing gradually while interacting with the ambient atmosphere, providing a material flux for film growth. In order to optimize this flux, the interaction must happen inside a vacuum chamber to avoid dispersion between the particles and the ambient air [15]. For some applications, it might be interested to collect these ablated particles on a particular surface. By doing this, the coating surface can have different properties from the original material: the object surface could become harder, noncorrosive, or conductive, while the rest of the object properties will remain practically the same [16–18].

Pulse laser deposition presents some serious advantages comparing to other techniques. First, it is very easy to implement, and the flexibility in terms of wavelength and power density allows the ablation of almost any material. Second, almost any geometry of the set-up can be chosen with a high degree of freedom because the laser beam is not part of the vacuum system [19]. Third, the use of a pulse laser enables a very precise control over the growth rate. Besides, due to the fact that this technique does not include impurities from the holder or the environment, it is a very clean technique [20]. And finally, the high kinetic energy of the ejected particles in comparison with other methods leads to an increase in the density of the layer and its adherence to the substrate [21]. However, the high laser energy involved in the process (which makes that microscopic or macroscopic particles can be ejected from the target) and an inhomogeneous distribution in the laser beam profile (and, in consequence, in the angular energy distribution) can cause an inhomogeneous layer with slightly different local densities in detriment to the desired properties of the film [22].

The attractive characteristics of PLD in the synthesis of multicomponent thin-film materials make it the perfect technique for a lot of applications [23, 24]. In some cases, it could be the synthesis of a thin-film material or structure [25]. In other cases, the research focused in the development of specific devices, such as in the growth of nitride films in the development of LED devices or in the fabrication of thin waveguiding films [26, 27]. PLD has also proven to be very effective in the growth of crystalline oxides, [28] or PLD-grown of high-temperature superconducting films (HTS), whose applications include high-frequency electronics for radio frequency, microwave communications, and superconducting quantum interference devices (SQUIDs) for the detection of magnetic fields [29]. In the area of wireless communication, radio frequency filters based on HTS thin films presents excellent results by reducing interference from out-of-band signals due to the low loss in the microwave frequency range for epitaxial oxide superconducting films in which PLD is extremely effective at production [30, 31]. Pulsed laser deposition has also played a key role in exploring more radical oxide device concepts, including various electric field-effect devices based on semiconducting oxide materials [32].

Selective laser elimination of thin materials from glass substrates presents some advantages in terms of time and material by being a relatively accessible and nonexpensive technique. While photolithography needs hours to fully fabricate the electrostimulator circuit, laser ablation can fully mark the same surface in a few minutes. Moreover, once the thin film of material is available, only the laser interaction is needed in order to fabricate the electrode, instead of all the chemical components. This technique uses the process of laser ablation, where the interaction of the laser energy with the sample leads to material removal. Usually, this phenomenon

depends on the absorption of laser photons by the sample material, which means that the wavelength of the laser has to be chosen carefully for the maximum absorption. However, the use of ultrafast lasers avoids this approach since ablation takes place as a result of multi-photon absorption at high peak intensities, which means that even materials normally transparent to the laser wavelength, which can be processed. In summary, laser ablation is a simple technique, which can be achieved with inexpensive optics and only requires any kind of beam or sample motion which can interface with CAD programs in order to mark complex patterns. The main problem presented is that the marked is limited to a small area, which is not even an issue if the goal is to work in a surface of a few square millimeters.

In this paper, we present a laser-based fabrication process for fabricating an electrostimulator on a 1 micron aluminum film deposited by PLD over a soda-lime glass. By using laser techniques, the aluminum is selectively removed to obtain a pre-designed electric circuit. In order to avoid direct contact between the circuit and the cell culture, a 100 μm glass is placed between them. Section 2 introduces materials and methods. In Section 3, we describe the electrical stimulator fabrication procedure and results, and Section 4 is devoted to discussion and conclusions.

## 2. Materials and methods

### 2.1. Laser set-up

The laser used in this experiment was a Rofin Power Line 20E operating at the fundamental wavelength of 1064 nm and a pulse with of 20 ns. The experimental set-up consists of a galvanometer system coupled to the laser source, with a flat field lens at the output with a spot size at focus of 15 μm. During the PLD process, the lens used has an effective focal length of 160 mm, providing a uniform distribution of irradiance in an area of $120 \times 120$ mm$^2$. For the ablation process, the selected lens has 100 mm of effective focal length, with an area of uniform distribution of irradiance of $80 \times 80$ mm$^2$.

### 2.2. Materials

The glass used as a substrate for fabricating the electrostimulator was a commercial soda-lime glass, provided by a local supplier. The composition of this glass (O 50.25%, Na 9.08%, Mg 2.19%, Al 0.54%, Si 33.08% and, Ca 4.87%) was determined by EDX analysis using a scanning electron microscope (SEM) Zeiss FESEM-ULTRA Plus. The material used for pulsed laser deposition of the thin film was an aluminum target of dimensions (10 cm $\times$ 10 cm $\times$ 1 mm) with a purity of 99.98%, provided by Goodfellow.

### 2.3. Thin layer deposition

Before PLD deposition, a six-step cleaning process was used for cleaning glass substrates. The samples were first brush-scrubbed in an aqueous and soap bath. They were then ultrasonically pulsed in a second deionized water and soap bath heated to 35°C for 30 minutes. Then, the water was changed and the process repeated. The fourth and fifth baths contained isopropyl

alcohol, heated to 35°C for 30 minutes. Finally, the samples were dried using air pressure. Once the cleaning process of the glass substrate was finalized, aluminum layers in the range of 600 nm to 1 m were deposited by PLD on the soda-lime substrate.

### 2.4. Characterization methods

The chemical composition of the soda-lime glass was determined by using a scanning electron microscope (SEM) Zeiss FESEM-ULTRA Plus issued with EDX analysis. The optical transmission of glass substrate was measured using a Perkin Elmer Spectrometer (type Lambda 950 UV/Vis). Fabricated samples were examined using an optical microscope Nikon MM-400. The characterization of the transmission spectrum across the sample was made using a BLUE-Wave Miniature Spectrometer, from Stellarnet Inc., which can measure in the range from 250 to 1150 nm. The characterization of the topographic profile was made using a Dektak3 profilometer from Veeco.

The electrical characterization of the electrostimulator is made using a Tektronix MSO 1 GHz 5GS/s oscilloscope. The oscilloscope was connected to a coil placed on a 100 μm glass over the surface of the circuit, in order to check if the electrical field is strong enough to pass through the glass to induce an electrical current in the coil.

### 2.5. Software control and simulation

In order to estimate the intensity and the homogeneity of the electrical field above the electrostimulator, we used the software ANSYS Maxwell. This program was used to simulate the parameters of the circuit and measure the electrical field in different planes over the surface of the circuit. The hardware selected for applying electrical signals to the electrostimulator is the NI USB-6501 portable digital I/O device, from National Instruments. It provides 5 V by default and up to 8.5 mA. The hardware was programmed using LabVIEW, from National Instruments, to apply a square signal whose parameters can be chosen by the final user to stimulate cells.

## 3. Results

The soda-lime glass samples were covered with an aluminum layer using a PLD process, and then the electrical tracks were fabricated by selective elimination of the thin metal film. **Figure 1** shows the diagram of the PLD process used in this work. The vacuum chamber was custom fabricated by Trinos Vacuum-Projects. It has a primary pump, which can provide a simple vacuum of $10^{-4}$ mbar and a secondary turbomolecular pump, which can achieve a high vacuum of $10^{-6}$ mbar.

**Figure 1** illustrates the vacuum chamber experimental set-up. The laser source is coupled to a source galvanometer head, with a flat field lens at the output of effective focal length 160 mm and a spot size at focus of 15 μm. The laser beam is focused on the surface of an aluminum layer placed at 45° (see **Figure 1a**). The glass substrate is placed in front of the target, parallel to it, and separated by 1 cm. The optimal pressure inside the vacuum chamber is $4 \times 10^{-5}$ mbar.

One of the most significant characteristics of the PLD technique is the high kinetic energy of the ejected particles. By raising this energy, the density of the layer increases and the adherence between the particles and the substrate improves. However, one of its problems is the high directionality of the ejected particles, which leads to an inhomogeneous density of the layer. This deposition, in the case of the PLD technique, follows a distribution with the form of $\cos^n\theta$, where $\theta$ is the angle between the direction of the ejected particles and the normal to the surface of the target, and n is a number depending on the conditions of the experiment, which can achieve values higher than 30 [20]. To solve this, inconvenient small area of the target (28 × 2 mm) were scanned with the laser beam instead of focussing it in a fixed point.

As consequence of these issues, rising the distance between the target and the substrate the homogeneity of the layer increases, so it is necessary to find the optimal separation in order to have a dense but homogeneous layer. After performing experiments over 60 samples, we have identified the optimal deposition parameters for laser operating at a fluence of 121 J/cm$^2$, while marking rectangles of 28 × 2 mm, with a separation between the target and the substrate of 1 cm, and with a combination of frequency and scan speed according to **Table 1**.

**Figure 2** shows the microscope images of the samples selected in **Table 1** illustrating the edge between the base glass material and the aluminum tracks deposited using PLD.

As it can be seen in **Figure 2**, the homogeneity of the layers, in terms of aluminum particles covering, vary according to the frequency and scan speed. We can observe that the samples 2 and 4 are the most homogeneous and present a uniform distribution of aluminum particles

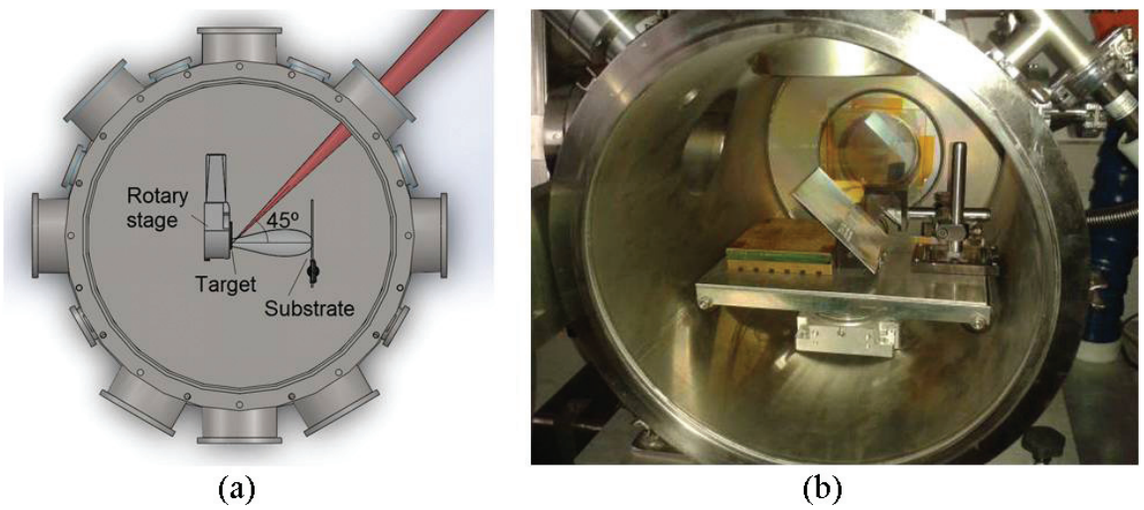


**Figure 1.** (a) Diagram of the PLD set-up for the fabrication process and (b) image of the PLD system.

| Sample | 1 | 2 | 3 | 4 |
|---|---|---|---|---|
| Repetition rate (KHz) | 1 | 5 | 7 | 3 |
| Scan speed (mm/s) | 50 | 250 | 350 | 150 |

**Table 1.** Ratio of frequency and scan speed.

http://dx.doi.org/10.5772/intechopen.70677

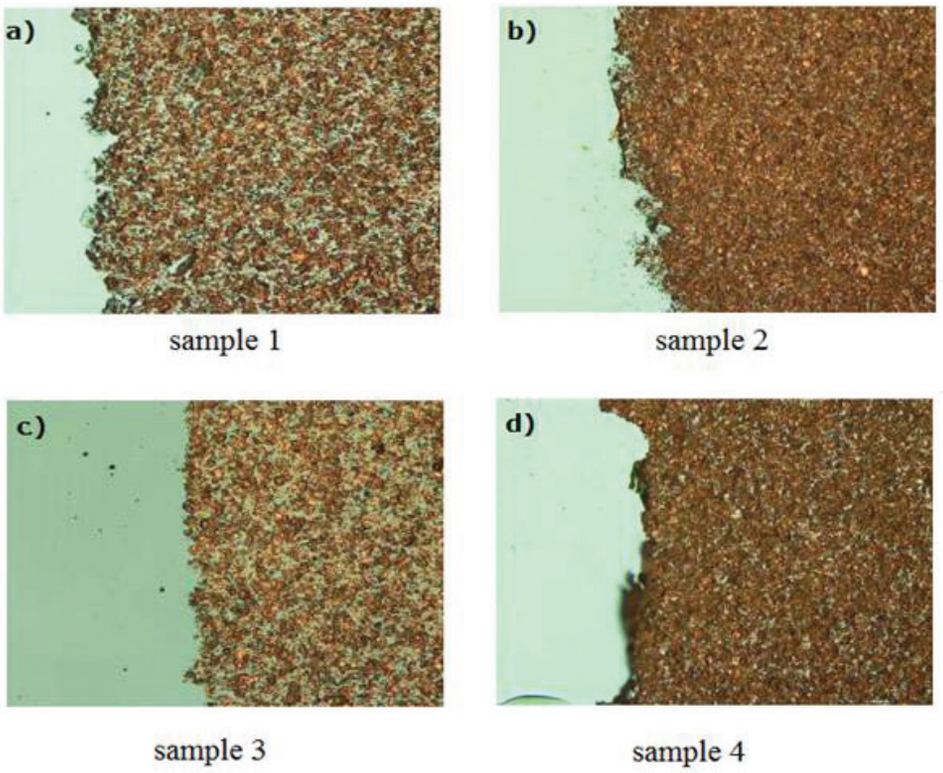


**Figure 2.** Microscope images of the deposited layers obtained with an objective 20×. (Each image corresponds with the laser parameters showed in **Table 1**).

along the surface. Conversely, **Figure 2a, c** shows spaces not covered by aluminum particles. The characterization of the transmission spectrum and the topographic profile of samples 2 and 4 are shown in **Figure 3**.

The percentage of light transmitted across the layer is shown in **Figure 3a, c**. In both cases, the percentage increases from the center to the borders of the aluminum layer due to the inhomogeneity of the deposition. In the central region, the layer is thicker than in the borders and reflects all the light. In **Figure 3b, d**, the topographic profile of the aluminum layer along a distance of 600 μm can be observed. The layer in the sample 2 shows an average height value of 1274 nm and a roughness average of 514 nm. The layer in the sample 4 shows an average height value of 653 nm and a roughness average of 389 nm. From now, the parameters of the sample 4 will be used, due to its less roughness: laser fluence of 121 J/cm$^2$, frequency of 3 KHz, scan speed of 150 mm/s, while marking rectangles of 28 × 2 mm, and with a separation between the target and the substrate of 1 cm.

### 3.1. Laser selective thin film removal

The laser direct-write technique for fabricating the electrostimulator system is based on the ablation of an aluminum layer deposited over the soda-lime glass substrate using a physical vapor deposition method. The laser set-up for selective aluminum layer removal is described in Section 2.1. The beam spot size was estimated to be 15 μm. For fabricating the

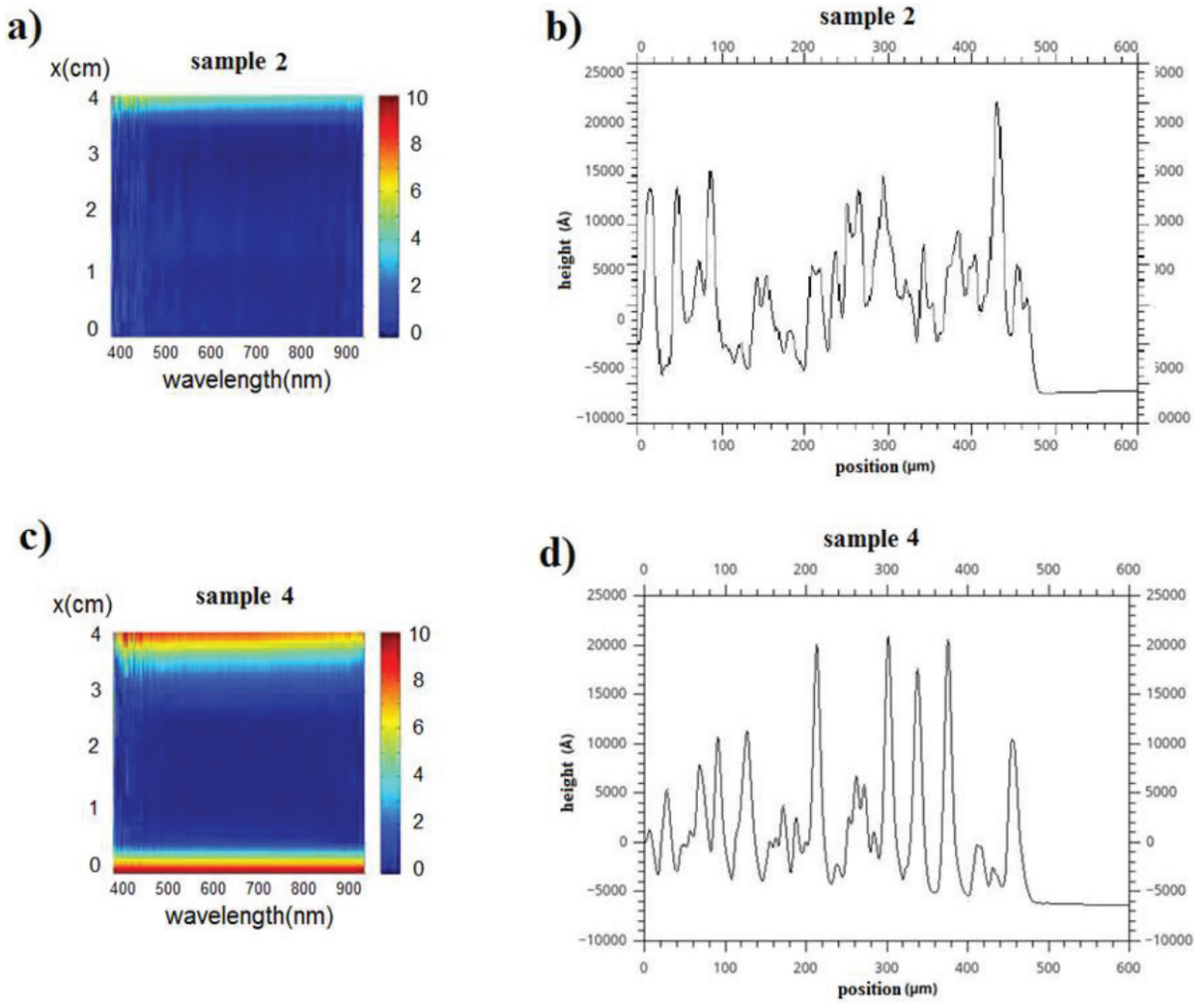


**Figure 3.** (a) Spectrum of the transmitted light across the layer in sample 2, (b) topographic profile of the surface of the layer in sample 2, (c) spectrum of the transmitted light across the layer in sample 4, and (b) topographic profile of the surface of the layer in sample 4.

electrical stimulator, the laser beam is focused on the top of the 1 micron aluminum layer deposited at the top of the glass substrate. **Figure 4a** shows the laser set-up for fabricating the electrostimulator. **Figure 4b** shows the CAD design used to fabricate the electrical stimulator. The laser parameters used were: average power 1.3 W, repetition rate 16 kHz, and scan speed 60 mm/s.

At laser fluence value below the damaged threshold of glass (920 J/cm$^2$) and above the ablation threshold of the target (2.4 J/cm$^2$), we were able to eliminate the aluminum layer selectively, according with the electrostimulator design (see **Figure 4b**). Strong interactions between the laser beam, the plasma, and the aluminum layer take place below the ablation threshold of soda-lime glass, resulting in high-quality elimination of the aluminum layer.

The calculations for determining applied threshold fluence ($\phi_{th}$) and ($\phi_0$) are obtained according to the method of Liu et al. [27]. The spatial fluence, ($\phi(r)$) for a Gaussian beam is given by:

http://dx.doi.org/10.5772/intechopen.70677

$$\phi(r) = \phi_0 e^{-2r^2/\omega_0^2} \tag{1}$$

where $\phi_0$ is the peak fluence in the beam, r is the distance from the centre of the beam, and $\omega_0$ is the Gaussian spot radius ($1/e^2$). The maximum fluence and the pulse energy, $E_p$, are related by:

$$\phi_0 = \frac{2E_p}{\pi\omega_0^2} \tag{2}$$

The peak fluence is related to the diameter of the ablated spot

$$D^2 = 2\omega_0^2 \ln\left(\frac{\phi_0}{\phi_{th}}\right) \tag{3}$$

where $D^2$ is the maximum diameter of the damaged region zone. It is possible to determine the beam radius using the value for $\omega_0$ from the plot of $D^2$ versus the logarithm of the pulse energy. Once $\omega_0$ is calculated, fluence values can then be found using Eq. (3). By plotting $D^2$ versus the natural log of the applied laser fluence and extrapolating the $D^2$ line to zero, $\phi_{th}$ can be calculated.

Due to the thinness of the aluminum layer, it is necessary to determinate the appropriate laser parameters, which allow to ablate the aluminum without causing damage in the glass substrate. These parameters are the fluence of the beam, the frequency of the pulses, and the speed of the spot along the sample. In order to determinate the ratio between the frequency and the speed, we calculated the degree of pulse overlap between the consecutive spots. This factor is set in the next equation

$$O_d = 1 - \frac{v}{2\omega f} \tag{4}$$

where $v$ and $f$ are the speed and frequency, and $\omega$ is the width of the spot, in this case 15 μm. Pulse overlapping is a crucial parameter for fabricating a homogeneous electrical track. Too

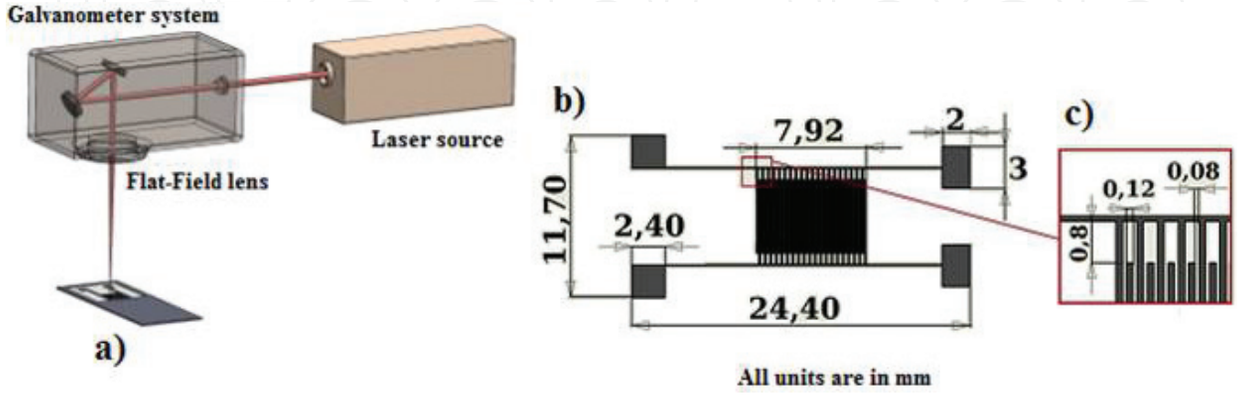


**Figure 4.** (a) Laser set-up for aluminum layer ablation, (b) electrostimulator design, and (c) extended view of the tracks dimensions.

overlapping will deliver too much energy over the glass, resulting on damage at surface, while low overlapping will result on inefficient material removal. In **Figure 5** are presented some samples of tracks of a 200 nm aluminum layer ablated with different frequencies (10, 12, and 14 KHz) and scan speeds (60 and 100 mm/s), and therefore with different pulse overlapping.

In **Figure 5**, we can observe different tracks created by the laser at different pulse overlapping. All of them were made with a power of 700 mW. Results show how the ratio of 12 KHz and 60 mm/s is the one with the most regular track in terms of width, with an overlap degree of 0.66. In other cases, the pulses are either too separated or too overlapped. Based on the above mentioned results, electrical tracks were fabricated using an overlapping factor of 0.66.

In order to adjust the optimal ratio between power and frequency, different tracks were made with different values of these parameters. We measured the diameter of the tracks related to the energy of each pulse (**Figure 6**).

**Figure 6** shows the diameter of the mark after ablation of a single line related to the energy per pulse, obtained by using different combinations of frequency (6–20 KHz) and power (700–2000 mW), where it can be observed the linear relation between the width of the line and the energy per pulse. This width will be taking into account during the aluminum layer removal process. Selected parameters were: Pulse energy: 90 μJ (which correspond to a frequency of 12 KHz, a power of 1.05 W) and a scan speed of 60 mm/s.

In **Figure 7**, you can see microscope images with the result of fabricating the electrostimulator with the previous parameters. The desired aluminum was successfully removed, without interferences between the tracks. Besides, the glass substrate has not been damaged. Tracks have an average length of 60.4 μm and are separated by a distance of 135 μm.

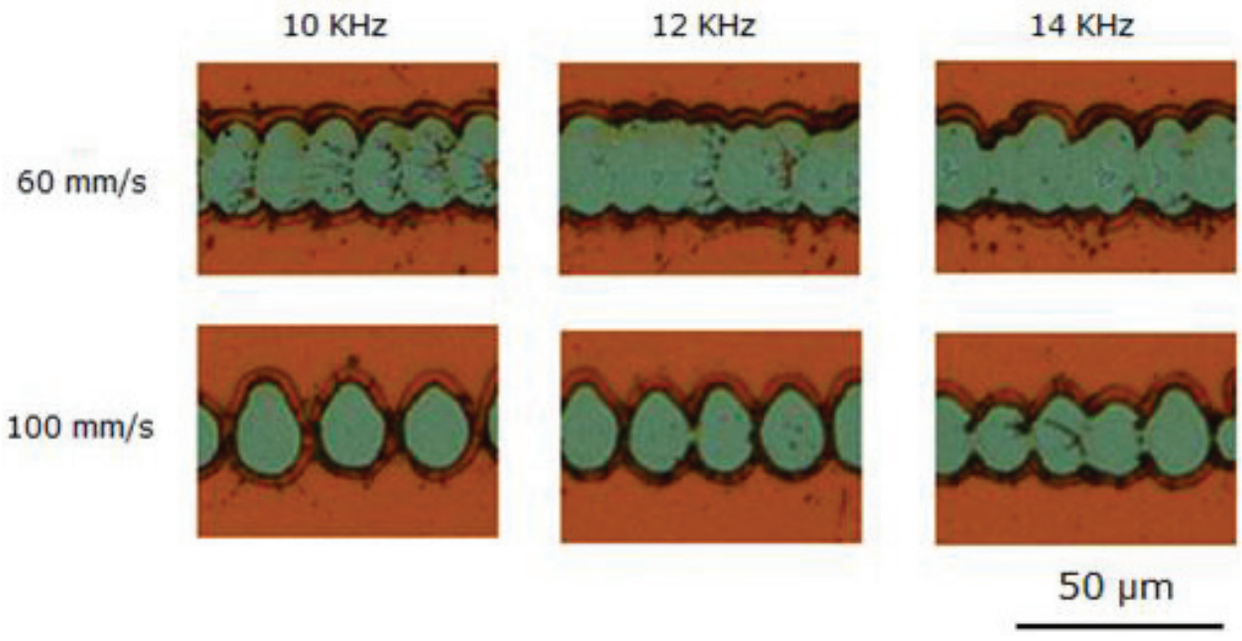


**Figure 5.** Aluminum layer ablated with different frequencies and scan speeds (thickness: 600 nm).

http://dx.doi.org/10.5772/intechopen.70677

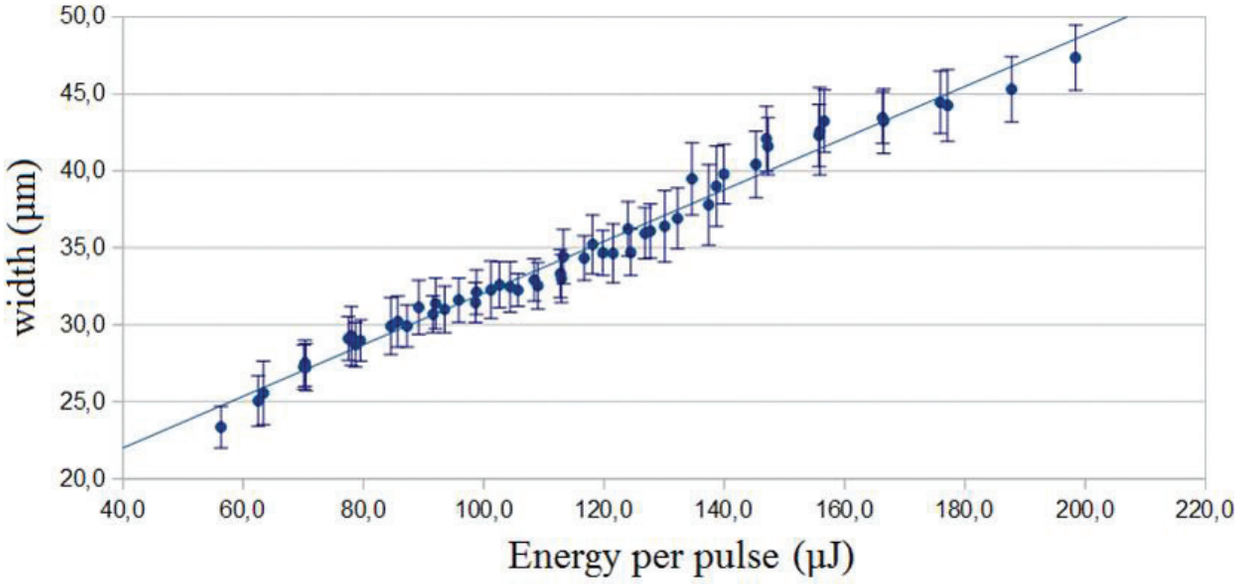


**Figure 6.** Diameter of the laser mark related to the energy per pulse.

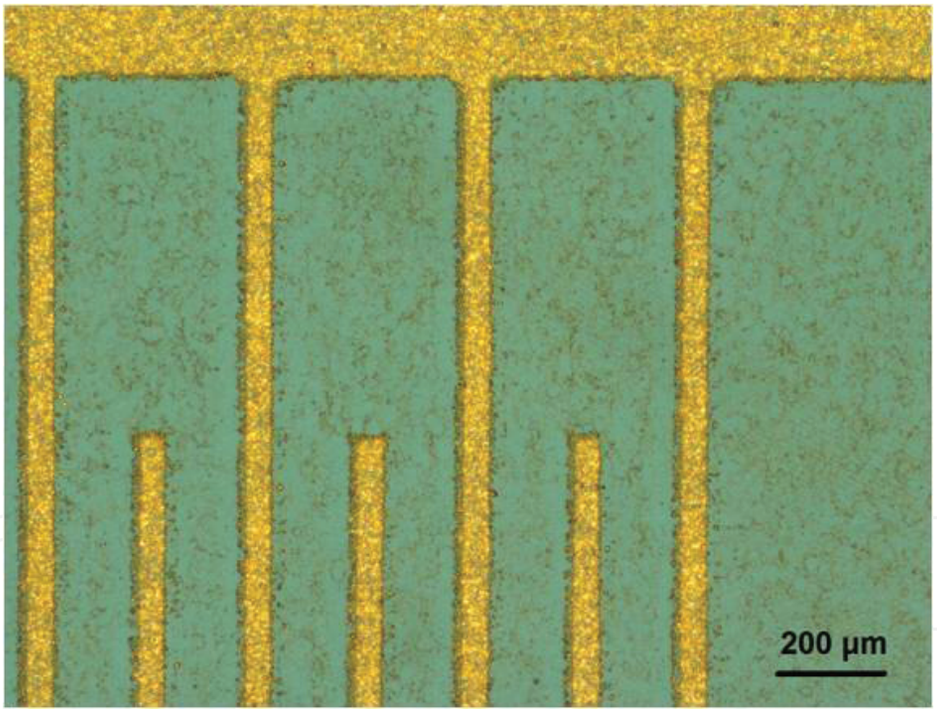


**Figure 7.** Microscope image of the electrical tracks after selective laser removal.

Motivated to maintain a lab-on-a-chip configuration for medical applications, we have created a culture chamber where performing the electrical characterization of fabricated electrical tracks. A polydimethylsiloxane layer (PDMS, Sigma-Aldrich, Saint Louis, MO) was cut from a PDMS-casted layer and placed on the top of the electrical stimulator (**Figure 8a**). Layer dimensions are 40 × 30 × 10 mm, with a hole of 10 × 8 mm. The glass cover slip (thickness: 100 µm) was placed on the top of the electrical tracks to avoid any contamination. Finally, these

elements are set between two polycarbonate layers, which will keep the device compact (**Figure 8b**).

Over the electrostimulator and the 100 μm glass is placed on a coil connected to an oscilloscope. In the terminals of the electrostimulator is induced a square signal with 5 V and 1 Hz, which should induce another signal in the coil (**Figure 9**).

**Figure 9a** shows a peak voltage induced during the rise time from the low to the high level of the square signal. **Figure 9b** shows an upper view of the set-up. The LED on the right is connected to the margins of the electrostimulator to check that there are no cuts in the circuit. The linear dependence of the voltage peak induced in the coil on the voltage applied to the electrostimulator is presented in **Figure 9c**.

The electrical field induced by the electrostimulator was simulated using the ANSYS Maxwell software. In this simulation, a model of the aluminum circuit in which 5 V was applied between the two terminals was introduced. In order to compare the induced electrical field with and without the glass cover, a second simulation was made keeping the same design of

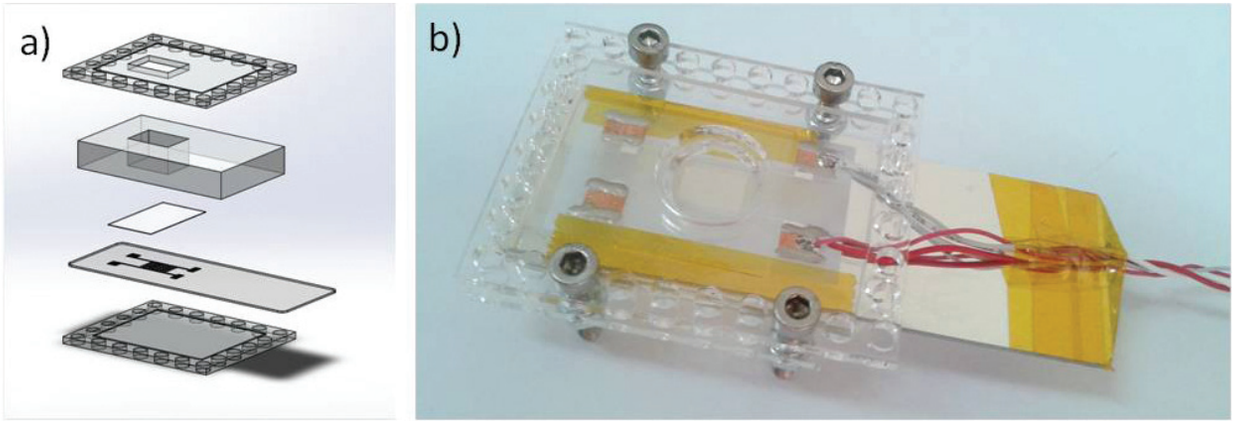


**Figure 8.** (a) Diagram of the elements of the electrostimulator and (b) picture of the final device.

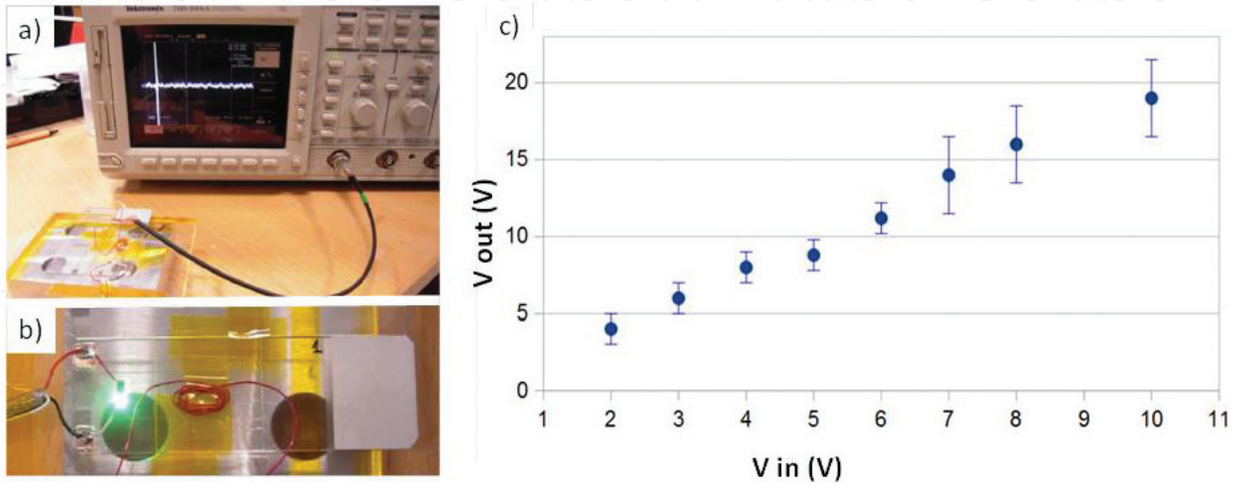


**Figure 9.** Set-up for checking the presence of an electric field generated above the glass.

http://dx.doi.org/10.5772/intechopen.70677

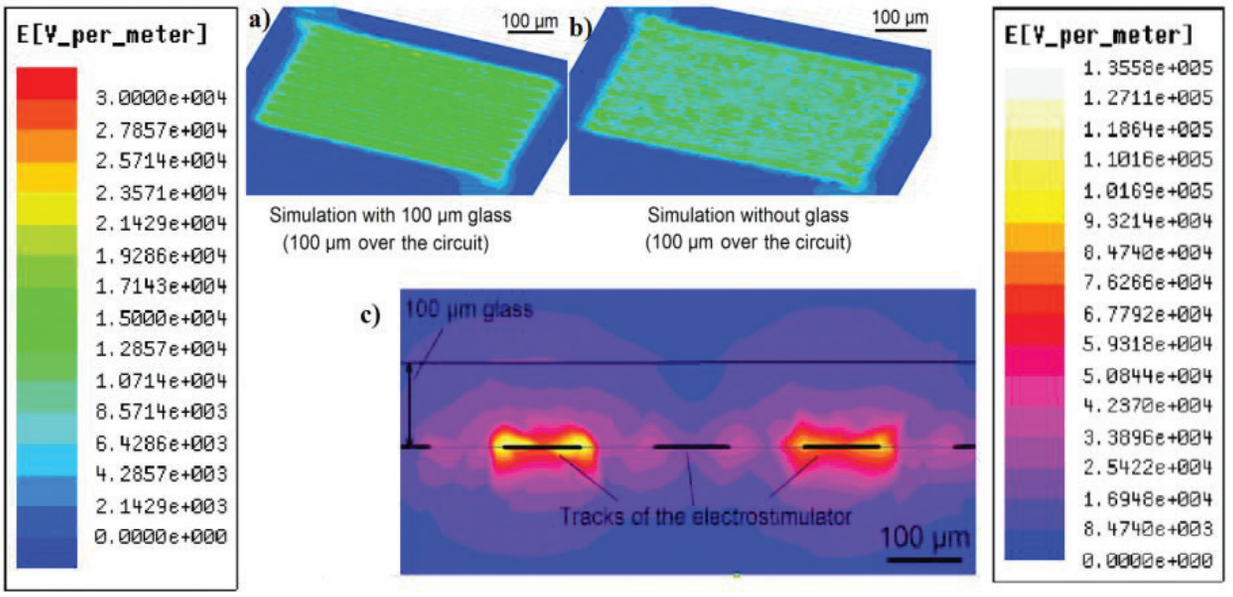


**Figure 10.** Simulation of the electric field generated above the electrostimulator with 5 V: (a) simulation with a 100 µm glass placed on the circuit, (b) simulation without 100 µm glass, and (c) cross sectional simulation of electrical tracks and glass.

the stimulator and parameters than the first one, but with a 100 µm glass over the electrostimulator. Results are shown in **Figure 10**.

In **Figure 10a, b**, the results show the electric field in a plane parallel to the electrostimulator, 105 µm above. In **Figure 10a**, a 100 µm glass is placed on the circuit, while in **Figure 10b** there is no glass at all. By comparing both results it can be observed that the mean value of the field when the glass is placed is about 1.4 x $10^4$ V/m, while in the case without the glass this value varies from 8 x $10^3$ V/m to 2 x $10^4$ V/m. The presence of the glass makes the electric field slightly weaker but much more homogeneous. As it was previously said, about $10^4$ V/m are needed to induce forces in the cell culture, so these results show that the electrical field generated is strong enough to interact with the cells.

## 4. Conclusions

By combining laser ablation techniques and pulse laser deposition, it fabricated an electrostimulator for medical applications. The layers resulting in the PLD process have been characterized by measuring transmission spectrum, by a profilometer, and by optical microscopy. Results show rough and homogeneous aluminum layers in the central region of the glass substrate. The circuit marked in the laser ablation process was characterized by an optical microscope, verifying that the aluminum was selectively removed without interference between the tracks and without damage in the substrate.

The electrical field generated by the device was simulated using ANSYS Maxwell, verifying that the field is able to pass through the glass with enough intensity to interact with the cells. The presence of the electrical field across the glass was also measured in an experimental way. As distinction regarding to other similar electrostimulator devices, the electrodes have been

isolated from the cell culture by using a thin soda-lime glass, solving biocompatibility issues between the material of the tracks and the cell culture.

## Acknowledgements

D. Nieto thanks to the Consellería de Cultura, Spain for his support under the Galician Program for Research Innovation and Growth (2011–2015) (I2C Plan). This work has been supported by the Xunta de Galicia under contract Agrupación estratéxica 2015–AEFIS AGRUP2015/11 (PC034).

## Author details

Angel Luis Aragón Beloso[1], María del Carmen Bao Varela[1], Alejandro Fernández Rodríguez[2], Gerard O'connor[3], Eliseo Pérez Trigo[4], Antonio Pazos Álvarez[4] and Daniel Nieto García[1,3]*

*Address all correspondence to: daniel.nieto@usc.es

1 Photonics4life Group, University of Santiago de Compostela, Santiago de Compostela, Spain

2 Superconducting Materials and Large Scale Nanostructures, Institut de Ciència de Materials de Barcelona (ICMAB-CSIC), Barcelona, Spain

3 NCLA/Inspire Labs, School of Physics, National University of Ireland, Galway, Ireland

4 Experimental High Energy Physics Group, University of Santiago de Compostela, Santiago de Compostela, Spain

## References

[1] Hankey GJ, Pomeroy VM, King LM, Pollock A, Baily-Hallam A, Langhorne P. Electrostimulation for promoting recovery of movement or functional ability after stroke. Stroke. 2006;**37**:2441-2442

[2] Dehail P, Duclos C, Barat M. Electrical stimulation and muscle strengthening. Annales de Readaptation et de Medicine Physique. 2008;**51**:441-451

[3] Boussetta N, Abeldelmalek S, Aloui K, Souissi N. The effect of neuromuscular electrical stimulation on muscle strength, functional capacity and body composition in haemodialysis patients. Biological Rhythm Research. 2017;**48**:157-174

[4] Archer S, Li T, Tudor A, Britland S, Morgan H. Cell reactions to dielectrophoretic manipulation. Biochemical and Biophysical Research Communications. 1999;**257**:687-698

[5] Tandon N, Cannizzaro C, Figallo E, Voldman J, Vunjak-Novakovic G. Characterization of electrical stimulation electrodes for cardiac tissue engineering. Conference Proceedings:

Annual International Conference of the IEEE Engineering in Medicine and Biology Society. 2006;**1**:845-848

[6] Tandon N, Cannizaro C, Chao P, Maidhoe R, Marsano A, Au H, Radisic M, Vunjak-Novakovic MG. Electrical stimulation systems for cardiac tissue engineering. Nature Protocols. 2009;**4**:155-173

[7] Tandon N, Marsano A, Cannizzaro C, Voldman J, Vunjak-Novakovic G. Design of electrical stimulation bioreactors for cardiac tissue engineering, In: Conference Proceedings: Annual International Conference of the IEEE Engineering in Medicine and Biology Society. 2008: pp. 3594–3597

[8] Geremia NM, Gordon T, Brushart TM, Al-Majed A, Vergea VMK. Electrical stimulation promotes sensory neuron regeneration and growth-associated gene expression. Experimental Neurology. 2007;**205**:347-359

[9] Abad-Villar EM, Kubáň P, Hauser PC. Determination of biochemical species on electrophoresis chips with an external contactless conductivity detector. Electrophoresis. 2005;**26**:3609-3614

[10] Woolley AT, Sensabaugh GF, Mathies RA. High-speed DNA genotyping using microfabricated capillary array electrophoresis chips. Analytical Chemistry. 1999;**69**:2181-2186

[11] Voldman J. Electrical forces for microscale cell manipulation. Annual Review of Biomedical Engineering. 2006;**8**:425-454

[12] Yafouz B, Kadri NA, Ibrahim F. Microarray Dot electrodes utilizing dielectrophoresis for cell characterization. Sensors. 2013;**13**:9029-9046

[13] Eason R. Pulsed Laser Deposition of Thin Films: Applications-Led Growth of Functional Materials. Hoboken, New Jersey: John Wiley & Sons, Inc.; 2006

[14] Krebs HU et al. Pulsed laser deposition (PLD)–A versatile thin film technique. Advances in Solid State Physics (Springer). 2003;**43**:505-517

[15] Ojeda A, Schneider CW, Lippert T, Wokaun A. Pressure and temperature dependence of the laser-induced plasma plume dynamics. Journal of Applied Physics. 2016;**120**:225301

[16] Jenniches H, Shen J, Mohan CV, Sundar Manoharan S, Barthel J, Ohresser P, Klaua M, Kirschner J. Structure and magnetism of pulsed-laser-deposited ultrathin films of Fe on Cu.(100). Physical Review B. 1999;**59**:1196-1207

[17] Shen J, Gai Z, Kirschner J. Growth and magnetism of metallic thin films and multilayers. Surface Science Reports. 2004;**52**:163-218

[18] Qiu Z, Gong H, Zheng G, Yuan S, Zhang H, Zhu X, Zhou H, Cao B. Enhanced physical properties of pulsed laser deposited NiO films via annealing and lithium doping for improving perovskite solar cell efficiency. Journal of Materials Chemistry C. 2017;**5**: 7084-7094 *Advance article*

[19] Koinuma H, Nagata H, Tsukahara T, Gonda S, Yoshimoto M. Ceramic layer epitaxy by pulsed laser deposition in an ultrahigh vacuum system. Applied Physics Letters. 1991;**58**:2027-2029

[20] Stafe M, Marcu A, Puscas N. Pulsed Laser Ablation of Solids, Springer Series in Surface Sciences. Vol. 53. Berllin Heidelberg: Springer-Verlag; 2014

[21] Warrender JM, Aziz MJ. Kinetic energy effects on morphology evolution during pulsed laser deposition of metal-on-insulator films. Physical Review B. 2007;**75**:085433

[22] Madsen NR, Gamaly EG, Rode AV, Luther-Davies B. Cluster formation through the action of a single picosecond laser pulse. Journal of Physics: Conference Series. 2007;**59**:762-768

[23] Rosales A, Castañeda-Guzmán R, de Ita A, Sánchez-Aké C, Pérez-Ruiz SJ. Detection of zinc blende phase by the pulsed laser photoacoustic technique in ZnO thin films deposited via pulsed laser deposition. Materials Science in Semiconductor Processing. 2015;**34**:93-98

[24] Kudyakova VS, Shishkin RA, Elagin AA, Baranov MV, Beketov AR. Aluminium nitride cubic modifications synthesis methods and its features. Review. Journal of the European Ceramic Society. 2017;**37**:1143-1156

[25] Lowndes D, Geohegan DB, Puretzky AA, Norton DP, Rouleau CM. Synthesis of novel thin-film materials by pulsed laser deposition. Science. 1996;**273**:898-903

[26] Li G, Wang W, Yang W, Wang H. Epitaxial growth of group III-nitride films by pulsed laser deposition and their use in the development of LED devices. Surface Science Reports. 2015;**70**:380-423

[27] Jelinek M. Functional planar thin film optical waveguide lasers. Laser Physics Letters. 2012;**9**(2):91-99

[28] Wei X, Zhao R, Shao M, Xu X, Huang J. Fabrication and properties of ZnO/GaN heterostructure nanocolumnar thin film on Si (111) substrate. Nanoscale Research Letters. 2013;**8**:112-120

[29] Matthews J, Lee SY, Wellstood FC, Gilbertson AF, Moore GE, Chatraphorn S. Multi channel high-T/sub c/scanning SQUID microscope. IEEE Transactions on Applied Superconductivity. 2003;**13**:219-222

[30] Hontsu S, Sakatani T, Fujimaki A, Nishikawa H, Nakamori M, Kawai T. Mechanically tunable high-temperature superconducting microwave filter with large shift of resonant frequency. Japanese Journal of Applied Physics. 2001;**40**:L1148

[31] Hedge MS. Epitaxial oxide thin films by pulsed laser deposition: Retrospect and prospect. Journal of Chemical Sciences. 2001;**113**:445-458

[32] Ji Y, Qin C, Niu H, Sun L, Jin Z, Bai X. Electrochemical and electrochromic behaviors of polyanilinegraphene oxide composites on the glass substrate/Ag nano-film electrodes prepared by vertical target pulsed laser deposition. Dyes and Pigments. 2015;**117**:72-82